Electronic Supplementary Material (ESI) for Energy & Environmental Science.

Electronic Supplementary Information (ESI) for

A general approach to cobalt-based homobimetallic phosphide ultrathin nanosheets for highly efficient oxygen evolution in alkaline media

Xiaofen Xiao,‡ Chun-Ting He,‡ Shenlong Zhao, Jing Li, Wensheng Lin, Zhongke Yuan, You Zhang, Qiang Zhang, Shuangyin Wang, Liming Dai, Dingshan Yu**

X. Xiao,‡ J. Li, W. Lin, Z. Yuan, Y. Zhang, Prof. D. Yu*
Key Laboratory for Polymeric Composite and Functional Materials of Ministry of Education
Key Laboratory of High Performance Polymer-based Composites of Guangdong Province
School of Chemistry
Sun Yat-Sen University, Guangzhou 510275, China
E-mail: yudings@mail.sysu.edu.cn

Dr. C. T. He‡
MOE Key Laboratory of Bioinorganic and Synthetic Chemistry
Sun Yat-Sen University, Guangzhou 510275, China

S. Zhao
Laboratory for Nanosystem and Hierarchy Fabrication
National Center for Nanoscience and Technology, Beijing 100190, China

Prof. Q. Zhang
Beijing Key Laboratory of Green Chemical, Reaction Engineering and Technology,
Department of Chemical Engineering, Tsinghua University, Beijing, China

Prof. S. Wang
State Key Laboratory of Chem/Bio-Sensing and Chemometric
College of Chemistry and Chemical Engineering
Hunan University, Changsha, 410082, China

Prof. L. Dai*
Department of Macromolecule Science and Engineering
Case Western Reserve University, Ohio 44106 USA
E-mail: liming.dai@case.edu

Experimental details

Synthesis of Co-NS and CoM(M = Ni, Mn, Cu, Zn)-P-NS samples

Synthesis of Co-NS: Synthesis of Co-ZIF is similar to the reported method in the literature.[1] $Co(NO_3)_2 \cdot 6H_2O$ (0.546 g) was dissolved in methanol solution (15 mL) to form solution A and 2-methyl imidazole (0.616 g) was dissolved in methanol (15 mL) to form solution B. Subsequently, solution A was quickly added into solution B in 1 min followed by sonication for 15 min. The mixture was washed by methanol and then filtered using decompression filter to achieve pure ZIF-67 particles. Pure ZIF-67 particles were dispersed in methanol solution (15 mL) and mixed with solution A. The mixture was transferred to 50 mL Teflon-lined stainless-steel autoclaves and the reaction was kept at 120 ^{o}C for 1 h. The resultant product was rinsed by methanol several times and separated by decompressing filter, followed by subsequent drying under vacuum at room temperature for further use. Finally, the yellow powder product was collected (denote as Co-NS).

Synthesis of CoNi-NS: CoNi-NS was synthesized by a published procedure with some modification.[1] A similar protocol was used to synthesize CoNi-NS except that solution A is formed by mixing $Co(NO_3)_2 \cdot 6H_2O$ and $Ni(NO_3)_2 \cdot 6H_2O$ (Co:Ni = 40:1, 20:1, 4:1, 1:1, respectively, the total molar quantity was 1.88 mmol) in 15 mL methanol. The resulted precursors were denoted as CoNi(40:1)-ZIF, CoNi(20:1)-ZIF, CoNi(4:1)-ZIF and CoNi(1:1)-ZIF, respectively. The final products (CoNi-based intermediates) were denoted as CoNi(40:1)-NS, CoNi(20:1)-NS, CoNi(4:1)-NS and CoNi(1:1)-NS, respectively. Their color varies with the increase of the Ni content.

Synthesis of CoMn(20:1)-NS: The procedure is similar to the above-mentioned one for the CoNi-NS synthesis, except that the starting solution A was formed by dissolving $Co(NO_3)_2 \cdot 6H_2O$ (0.52 g) and $Mn(NO_3)_2 \cdot 6H_2O$ (0.0257 g) in 15 mL of methanol.

Synthesis of CoCu(20:1)-NS: The procedure is similar to the above-mentioned one for the CoNi-NS synthesis, except that the starting solution A was formed by dissolving $Co(NO_3)_2 \cdot 6H_2O$ (0.52 g) and $Cu(NO_3)_2 \cdot 3H_2O$ (0.0216 g) in 15 mL of methanol.

Synthesis of CoZn(20:1)-NS: The procedure is similar to the above-mentioned one for the CoNi-NS synthesis, except that the starting solution A was formed by dissolving $Co(NO_3)_2 \cdot 6H_2O$ (0.52 g) and $Zn(NO_3)_2 \cdot 6H_2O$ (0.0266 g) in 15mL of methanol.

Synthesis of CoP-NS or CoNi-P-NS: A quartz crucible loaded with 0.12 g of NaH_2PO_2 was placed at the upstream side of the tube furnace and the other quartz crucible loaded with 0.02 g of intermediates A (A is Co-NS, CoNi-NS, CoMn(20:1)-NS, CoCu(20:1)-NS or CoZn(20:1)-NS) was placed at the downstream side. After evacuation and N_2 (99.999%) pumping three times, the furnace temperature was elevated to 250 °C at a heating rate of 5 °C /min and held at 250 °C for 60 min, followed by raising the temperature to 300 °C at a heating rate of 10 °C /min and maintaining the temperature at 300 °C for another 60 min under N_2 flow at a flow rate of 60 sccm. The final products were obtained after cooling to ambient temperature under N_2 flow. The resultant black phosphide nanosheets are denoted as CoP-NS, CoNi(40:1)-P-NS, CoNi(20:1)-P-NS, CoNi(4:1)-P-NS, CoNi(1:1)-P-NS, CoMn(20:1)-P-NS, CoCu(20:1)-P-NS and CoZn(20:1)-P-NS, respectively. As control experiments, the phosphidation treatment of CoNi(20:1)-NS was conducted at 250 °C for 1 h and at 300 °C for another 20 min.

Synthesis of CoNi-ZIF-P: CoNi(20:1)-ZIF underwent direct phosphidation using the above mentioned method for the synthesis of CoNi(20:1)-P-NS. The resulted black powder was denoted as CoNi-ZIF-P.
Note: Here 1:0, 1:1, 40:1, 20:1, 4:1 and 1:1 represent the Co/M (M=Mn, Ni, Cu, Zn) molar ratios in CoM-ZIF precursors. And we only chose several typical examples for the presentation.

Structural characterization: Powder X-ray diffraction (XRD) patterns of the samples were recorded on a Bruke D8 Advance powder X-ray diffractometer with a Cu K source (λ= 0.15406 nm). 2-theta was run from 5 to 75^{o} with a scan speed of 0.25 ^{o}/s. The morphology and microstructure of the products were characterized by scanning electron microscopy (SEM, S4800) and transmission electron microscopy (TEM, JEOL JEM-2100FkV, FEI, operating at 200 kV). For TEM investigation, the samples were dispersed in ethanol by ultrasonication. A drop of suspension was then placed on a 200-mesh Cu grid support, while a Mo mesh is used for CoCu(20:1)-P-NS, which was dried in a vacuum oven at room temperature for 4 h. X-ray photoelectron spectroscopy (XPS) measurements were executed using an ESCALAB 250 instrument. Element composition was analyzed using a VISTA-MPX EL02115765 inductive coupled plasma atomic emission spectrometer (ICP AES). Atomic force microscopic measurements (AFM) for identifying the thin-film thickness was performed on a Bruker Multimode 8 system with an E-head (12.5 μm scanner) in tapping mode after depositing a drop of dispersion of the as-prepared samples of CoNi(20:1)P-NS onto the Si wafer and dried under room temperature. Nitrogen adsorption isotherms were collected on a Micromeritics ASAP 2020 system at 77 K. Prior to adsorption measurements, the samples were degassed at 200 ℃ for at least 10 h. Pore size distributions (PSD) were calculated using the adsorption branch of the isotherms; the resulting PSD curves defined as d*V*/d*D*, where *V* is the volume adsorption amounts and *D* is the pore width.

Density functional theory calculations

In the alkaline solution, the overall OER reaction was:

$$4\ OH^- \rightarrow O_2 + 2\ H_2O + 4\ e^-$$

And the electrocatalytic OER processes include four elementary steps:

$$OH^- \rightarrow OH^* + e^- \qquad (i)$$
$$OH^- + OH^* \rightarrow H_2O + O^* + e^- \qquad (ii)$$
$$OH^- + O^* \rightarrow OOH^* + e^- \qquad (iii)$$
$$OOH^* + OH^- \rightarrow O_2 + H_2O + e^- \qquad (iv)$$

The potential of the electro-catalytic OERs are dependent on the Gibbs free energies of these four elementary steps. According to the previous study,[2] the Gibbs free energy of each step was calculated as follow:

$$\Delta G = \Delta E + \Delta \mathrm{ZPE} - T\Delta S$$

Where ΔE is the reaction energy calculated using DFT. ΔZPE is the difference in zero point energies due to the reaction, and ΔS is the change in entropy calculated using vibrational frequencies analysis.

In this work, periodical models base on the CoP lattice was chosen. A vacuum of at least 12 Å is used to separate the slab from its periodic images. All the geometry optimizations and energy calculations were performed by the spin polarization density functional theory (DFT) method through the Dmol^3 procedure. The widely used generalized gradient approximation (GGA) with the Perdew-Burke-Ernzerhof (PBE) functional and the double numerical plus polarization (DNP) basis set were used for the non-metal atoms. An accurate DFT Semi-core Pseudopots (DSPP) was employed for the metal atoms. For all the DFT calculations, the energy, gradient and displacement convergence criterions were set as 1×10^{-5} Ha, 2×10^{-3} Å and 5×10^{-3} Å, respectively.

Electrode preparation and electrochemical tests

Preparation of catalysts ink: Typically, 3 mg of catalyst was suspended in a mixture of 250 μL of ethanol and 750 μL of deionized water with 50 μL of Nafion (5 wt %) solution to form a homogeneous catalyst ink by sonication for 40 min. Subsequently, 10 μL of catalyst ink was dropped onto the surface of rotating-disk-electrode by a micropipette followed by drying at room temperature. The loading amount of the catalyst is about 0.153 mg/cm^2.

Electrochemical measurements: All the electrochemical measurements were performed using a CHI 760 (CH Instruments Inc., Shanghai) electrochemical workstation equipped with a Pine Instrument (model AFMSRCE) in a typical three-electrode system with 1 M KOH as the electrolyte solution, a Pt plate as the counter electrode, and an HgO/Hg electrode as the reference electrode. Rotating disk electrode (RDE, Ø5 mm, Pine) covered with a thin catalyst film was used as the working electrode.

Potential reported in this work was expressed vs. RHE based on the standard calculation method:

$$E(\mathrm{RHE}) = E(\mathrm{HgO/Hg}) + 0.098 + 0.059\mathrm{pH}.$$

All tests were carried out in O_2 saturated 1 M KOH.

Linear-sweep voltammetry measurements were performed at a rotation speed of

1600 rpm at a scan rate of 10 mV s^{-1} to get rid of the bubbles. Cyclic voltammograms (CVs) were conducted at a rotation rate of 1600 rpm at a scan rate of 50 mV/S. Chronoamperometic plot of the sample was recorded at an applied overpotential of 0.28 V using an RDE electrode at a rotation speed of 1600 rpm in 1 M KOH. All polarization curves were iR corrected.

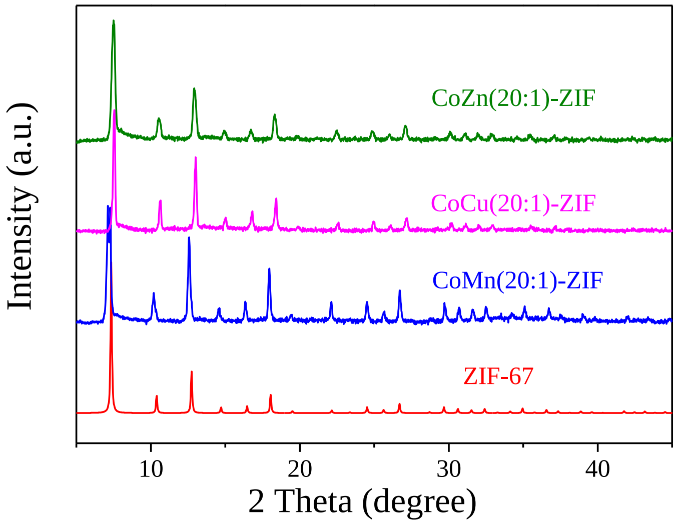

Figure S1. XRD patterns of CoM(20:1)-ZIF precursors (M = Mn, Cu, Zn).

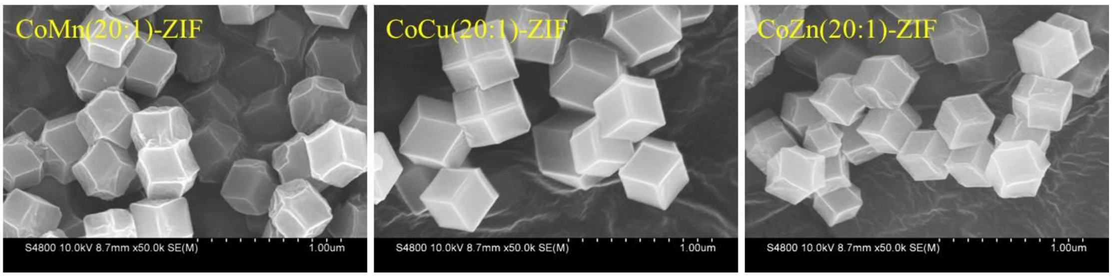

Figure S2. SEM images of CoM(20:1)-ZIF precursors (M = Mn, Cu, Zn).

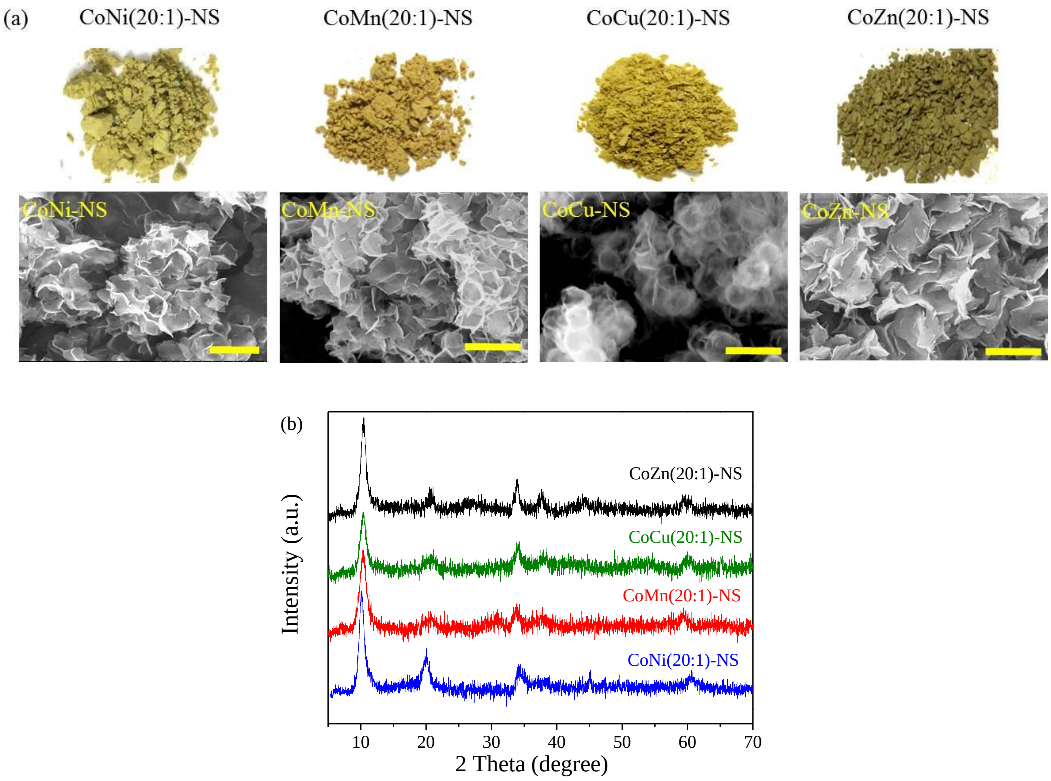

Figure S3. a) Optical photographs (Top) and the corresponding SEM images (Bottom) and b) XRD patterns of CoNi(20:1) -NS, CoMn(20:1)-NS, CoCu(20:1)-NS, and CoZn(20:1)-NS. (Scale bar, 1 μm)

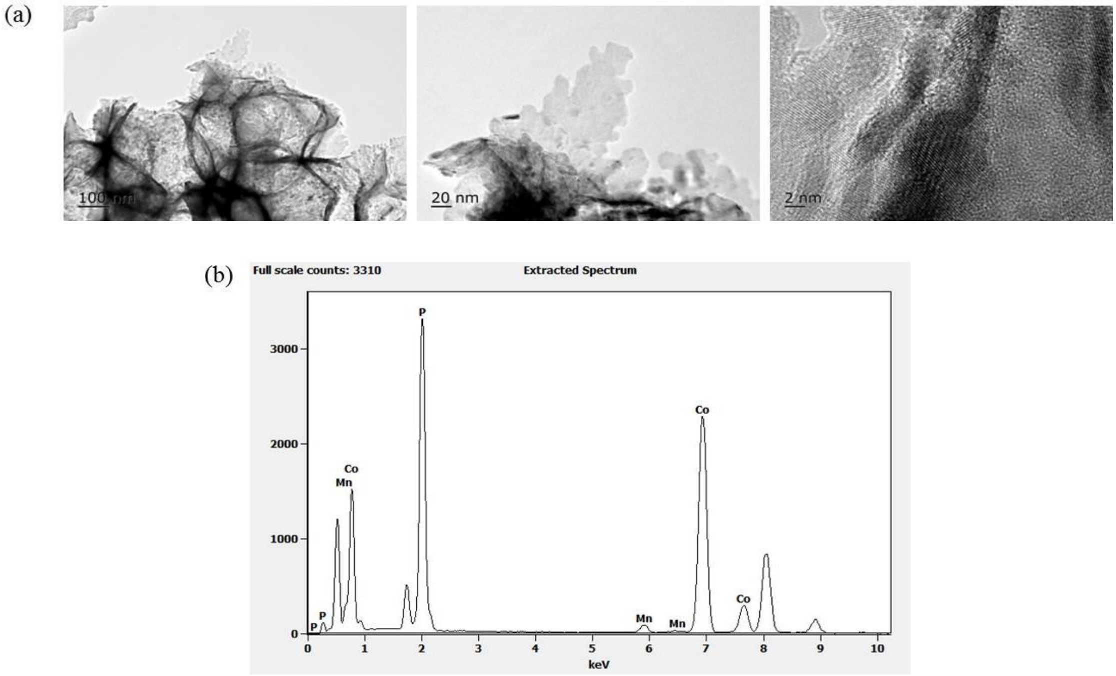

Figure S4. a) TEM images and b) EDX spectrum of the CoMn(20:1)-P-NS.

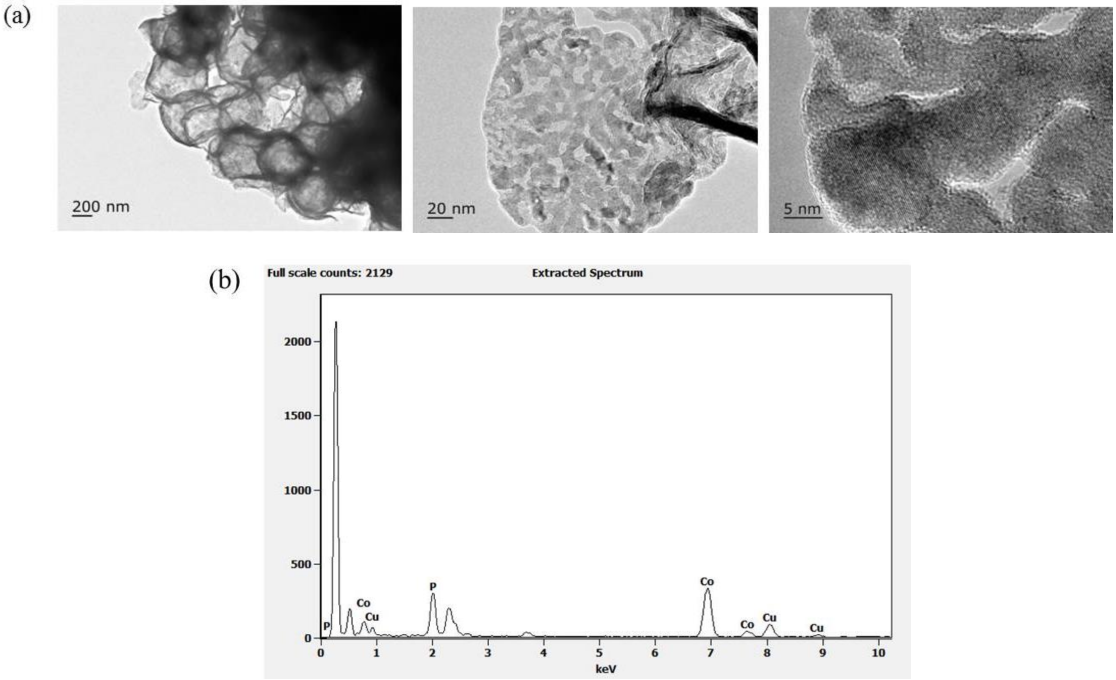

Figure S5. a) TEM images and b) EDX spectrum of the CoCu(20:1)-P-NS. (Mo mesh instead of Cu mesh is used as the substrate for EDX measurements)

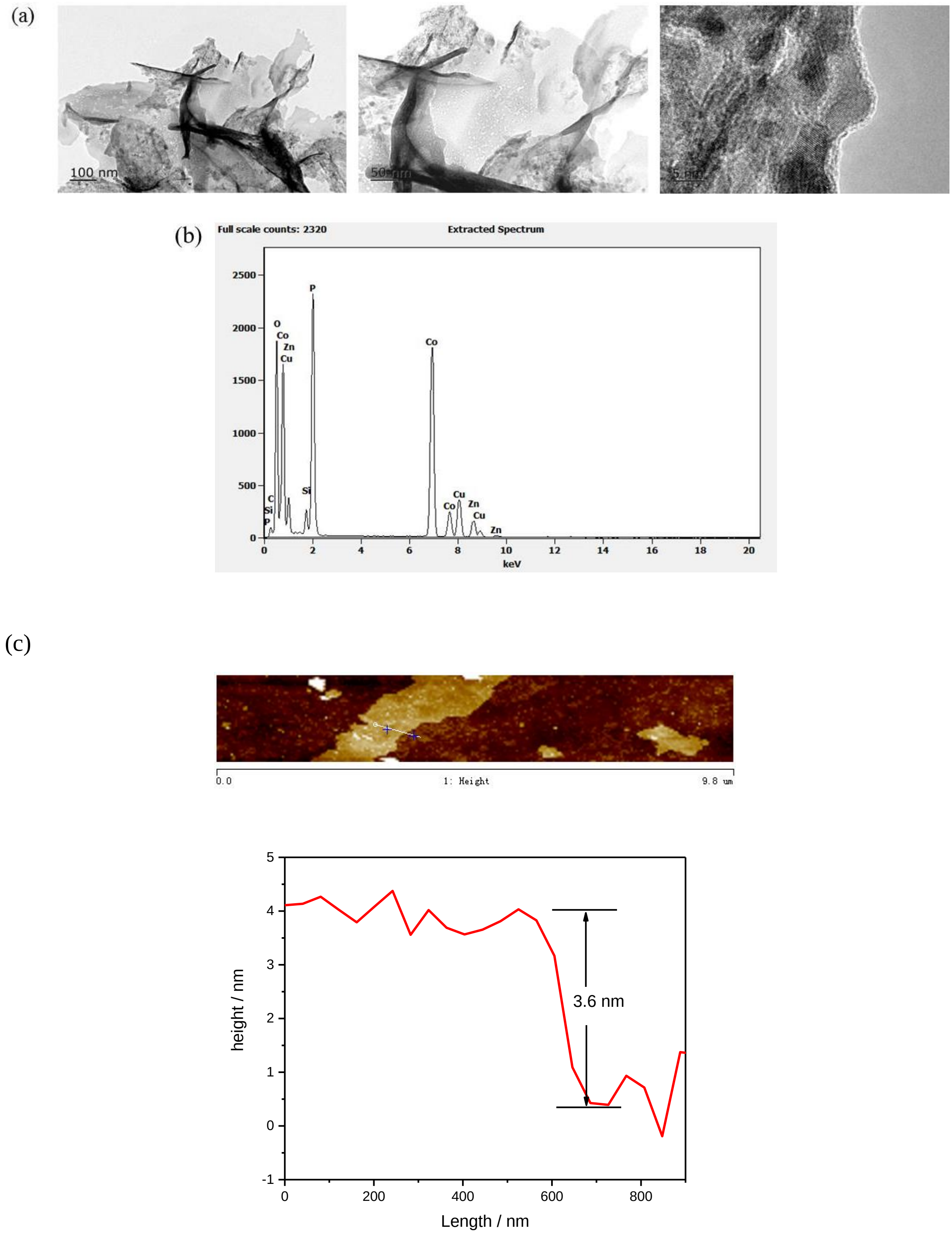

Figure S6. a) TEM images, b) EDX spectrum of the CoZn(20:1)-P-NS, and c) AFM image of the ultrathin CoNi(20:1)-P nanosheets.

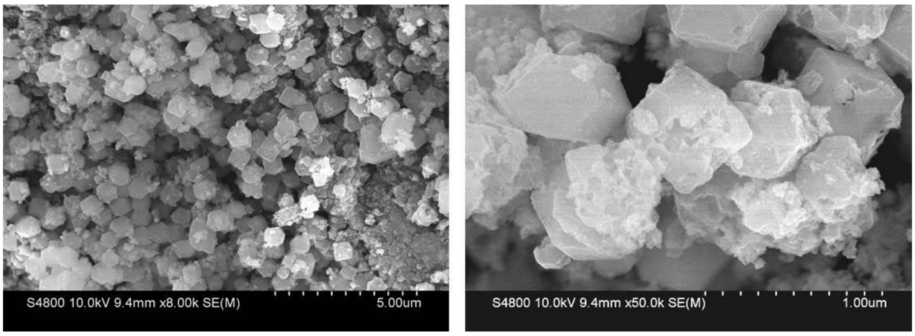

Figure S7. SEM images of CoNi(20:1)-ZIF-P by direct phosphidation of CoNi-ZIF at 250 ℃ for 1 h and at 300 ℃ for another 1 h.

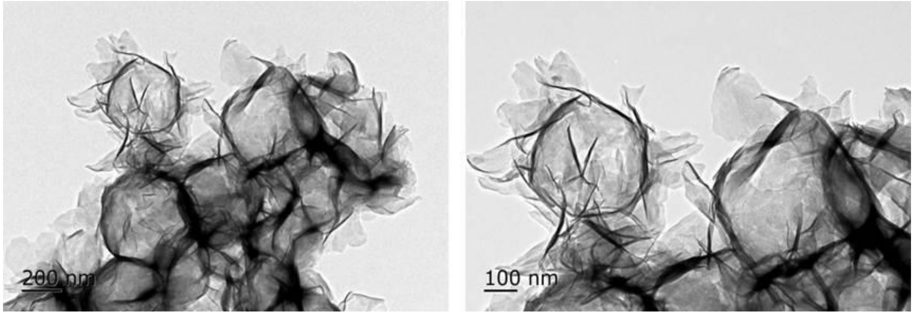

Figure S8. High-resolution TEM images of CoNi(20:1)-NS intermediates.

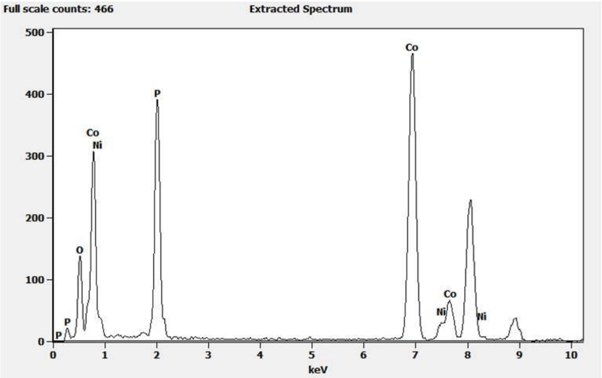

Element Line	Net Counts	Weight %	Atom %
P K	4357	30.76	45.81
Co K	8000	66.55	52.08
Ni K	321	2.69	2.11
Total		100.00	100.00

Figure S9. The EDX spectrum (left) and table of elements percentage (right) of the CoNi(20:1)-P-NS from STEM.

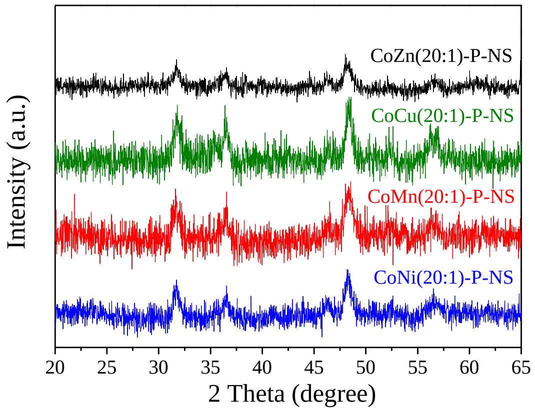

Figure S10. XRD patterns of CoMn(20:1)-P-NS, CoNi(20:1)-P-NS, CoCu(20:1)-P-NS and CoZn(20:1)-P-NS. The characteristic diffraction peaks at 31.6°, 36.3°, 46.2°, 48.1°, 52.3° and 56.8° can be indexed to the (011), (111), (112), (211), (103), (301) of CoP (JCPDS-29-0497). In particular, no new peaks arising from other metal phosphides or possible impurities are detected, and there is also no obvious shift for the diffraction peaks of M-doped CoP relative to pristine CoP. These results indicate that second metal ions (M = Ni^{2+}, Mn^{2+}, Cu^{2+}, Zn^{2+}) are indeed homogeneously doped into the crystal lattice of CoP and the doping nearly does not affect the lattice constant due to the similar ionic radius of guest and host metal ions.

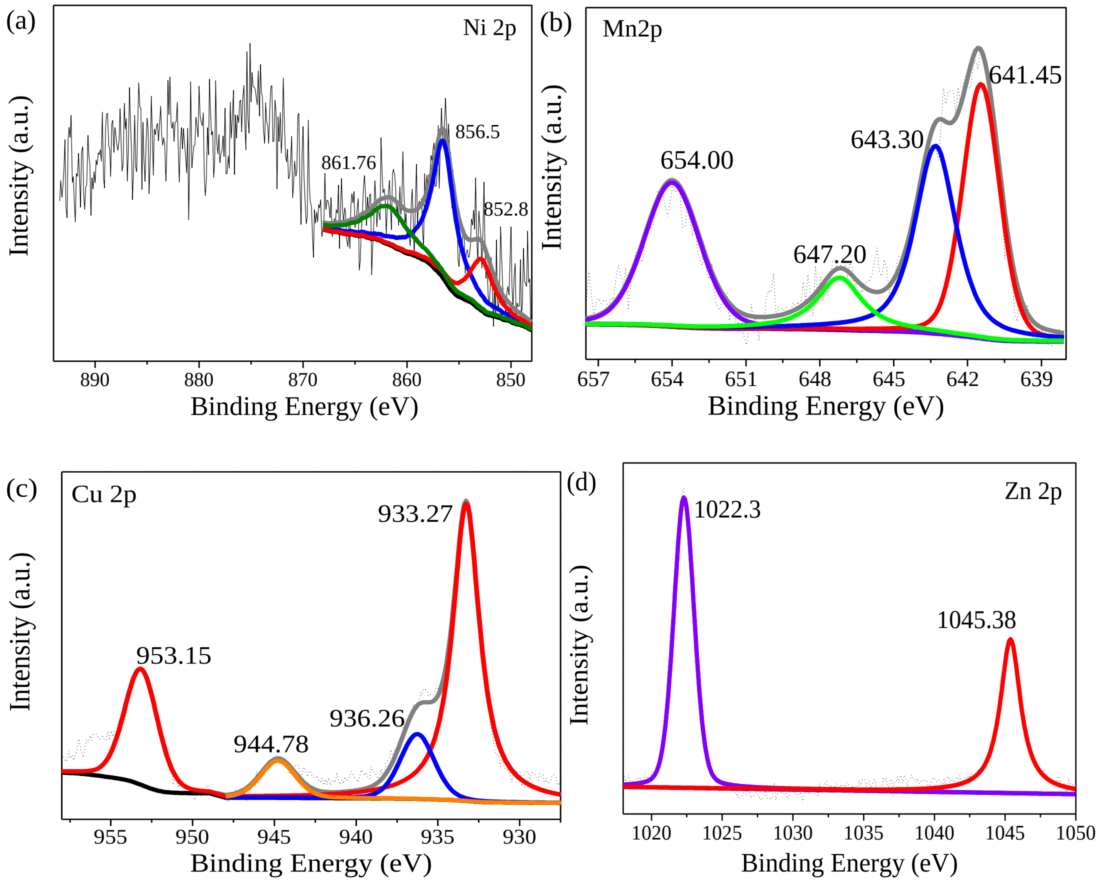

Figure S11. High-resolution XPS spectrum of a) Ni 2p for CoNi(20:1)-P-NS, b) Mn 2p for CoMn(20:1)-P-NS, c) Cu 2p for CoCu(20:1)P-NS, d) Zn 2p for CoZn(20:1)-P-NS.

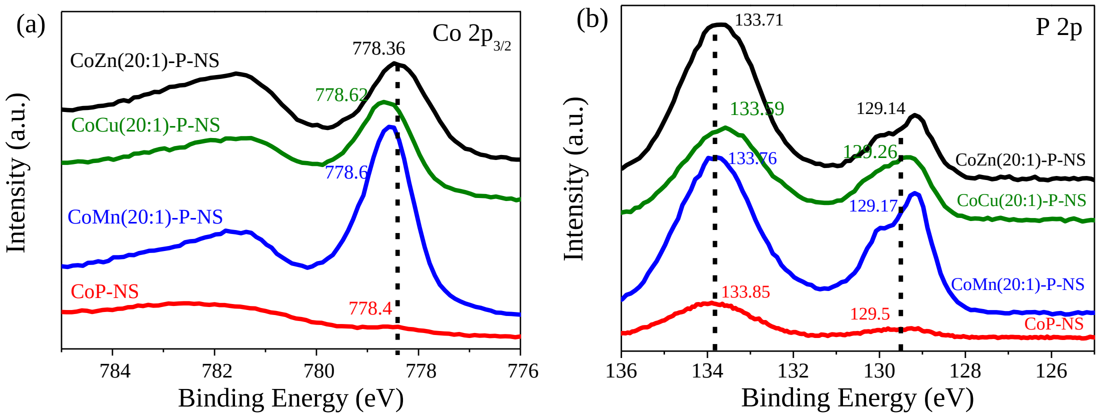

Figure S12. XPS spectra of a) Co 2p, b) P 2p in CoP-NS and CoM(20:1)-P-NS (M = Mn, Cu, Zn). Figure S16 presents the XPS spectrum of Co $2p_{3/2}$ and P $2p_{3/2}$ for CoP-NS and CoM(20:1)-P-NS (M = Mn, Cu, Zn). Compared with the peak centered at 778.4 eV assigned to Co $2p_{3/2}$ for CoP-NS, Co $2p_{3/2}$ for CoM(20:1)-P-NS (M = Mn, Cu, Zn) are shifted to 778.6 eV, 778.62 eV and 778.36 eV, respectively. The peak of P $2p_{3/2}$ for CoM(20:1)-P-NS (M = Mn, Cu, Zn) are shifted to 129.17 eV, 129.26 eV and 129.14 eV, respectively, as compared with the peak centered at 129.5 eV of P $2p_{3/2}$ for CoM(20:1)-P-NS. The shift of the peak positions could be caused by the second metal-doping into the CoP crystal lattice.

The XPS spectra were referenced to C 1s emission at 284.8 eV and fitted by Gauss type and the FWHM was constrained to < 3 eV, while the Lorentzian-Gaussian constant was set as 20 %.

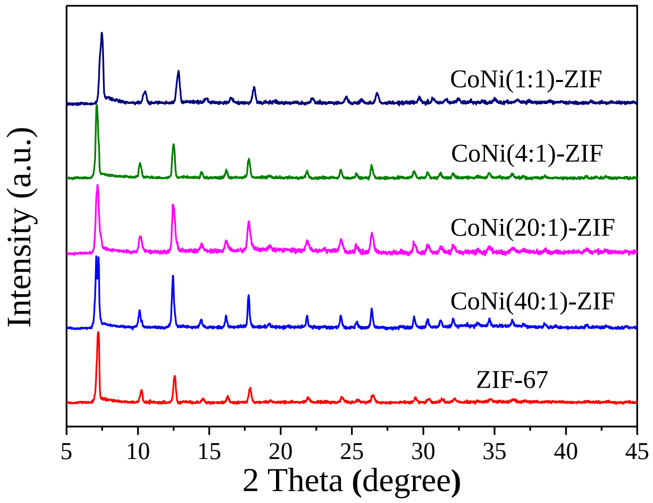

Figure S13. XRD patterns of CoNi-ZIF precursors with different Co/Ni ratios

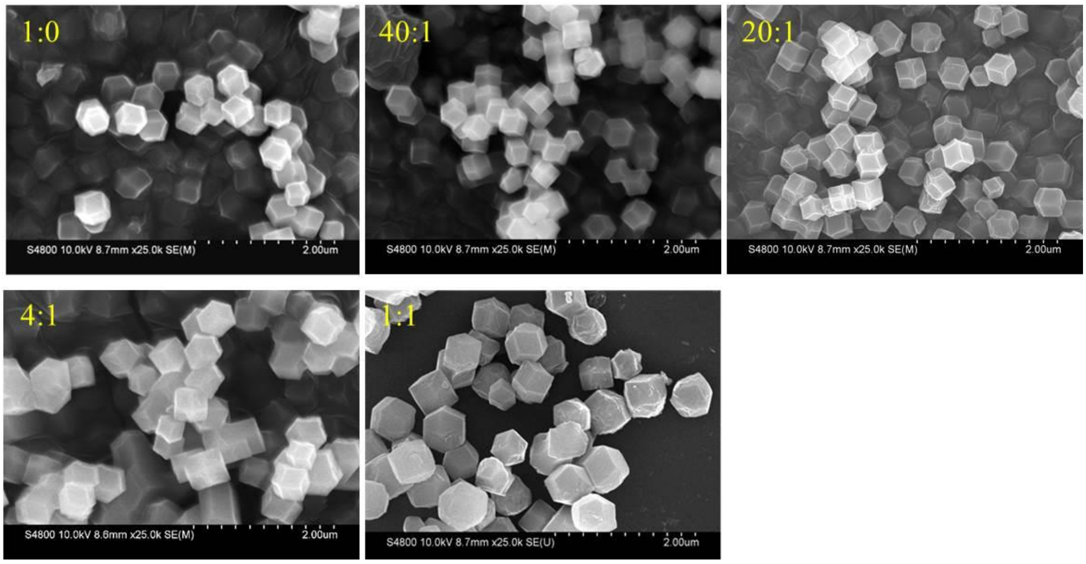

Figure S14. SEM images of CoNi-ZIF precursors with different Co/Ni ratios

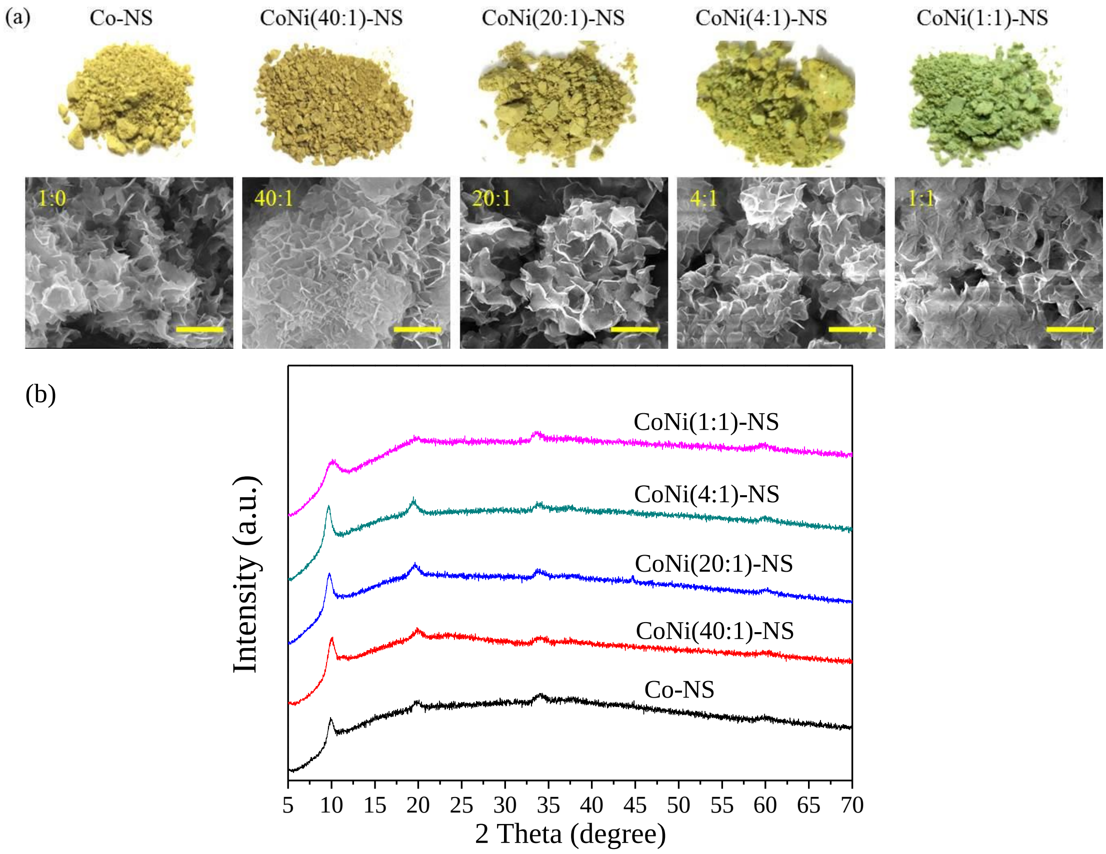

Figure S15. a) Optical photographs (Top) and corresponding SEM images (Bottom) and b) XRD patterns of Co-NS, CoNi(40:1)-NS, CoNi(20:1)-NS, CoNi(4:1)-NS and CoNi(1:1)-NS. (Scale bar, 1μm)

Note: 1:0, 40:1, 20:1, 4:1, 2:1 and 1:1 represent the Co/Ni ratios in the CoNi-ZIF starting precursor.

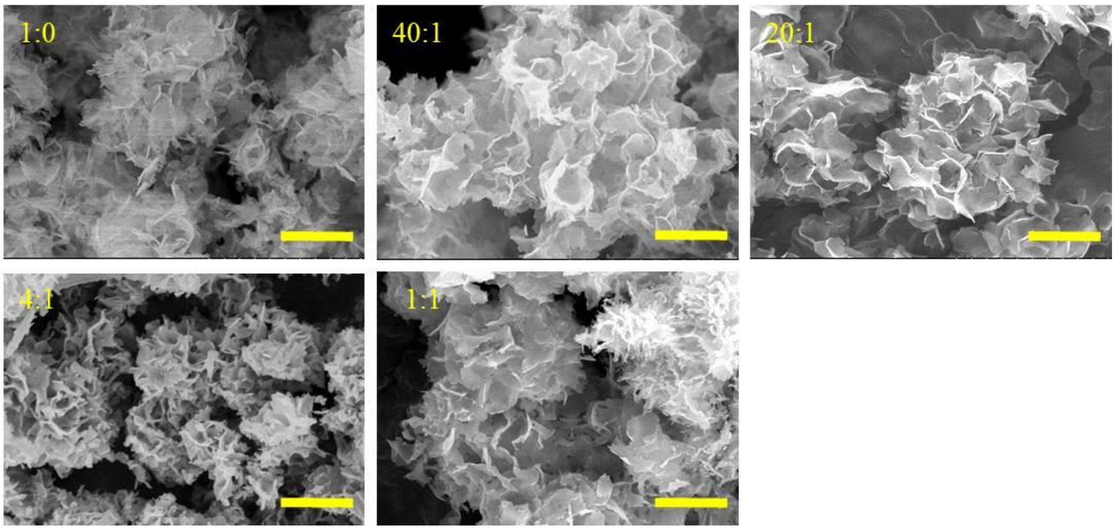

Figure S16. SEM images of CoNi-P-NS with different Co/Ni ratios in the starting precursors. (Scale bar, 1 μm)

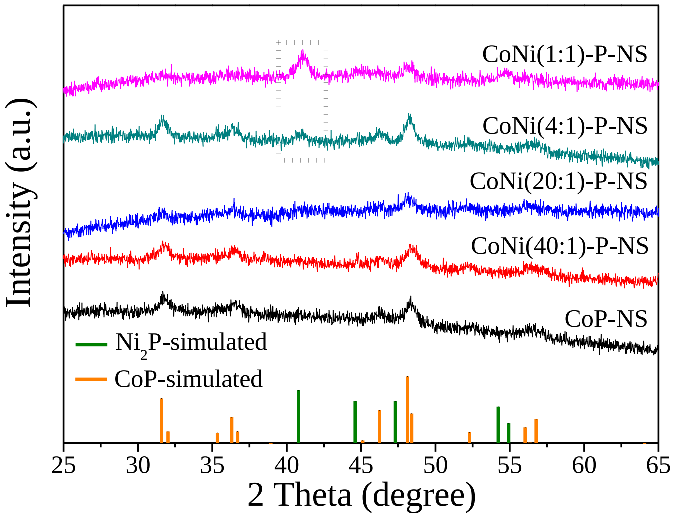

Figure S17. XRD patterns of CoP-NS and CoNi-P-NS with different Co/Ni ratios in the starting precursor. Different from those of CoNi(20:1)-P-NS and CoNi(40:1)-P-NS, a new diffraction peak at 40.8 ° appeared for the samples with the Co/Ni ratios of 4:1 and 1:1 in the starting precursors, which can be indexed to the (111) plane of Ni$_2$P (JCPDS-03-0953). These results suggest that, when the Ni content is too high, the phase segregation inevitably occurs due to the lattice mismatch during the phosphidation process. Note: actually, we have performed a series of experiments with different Co/Ni ratios. Here we only chose four representative samples for the presentation.

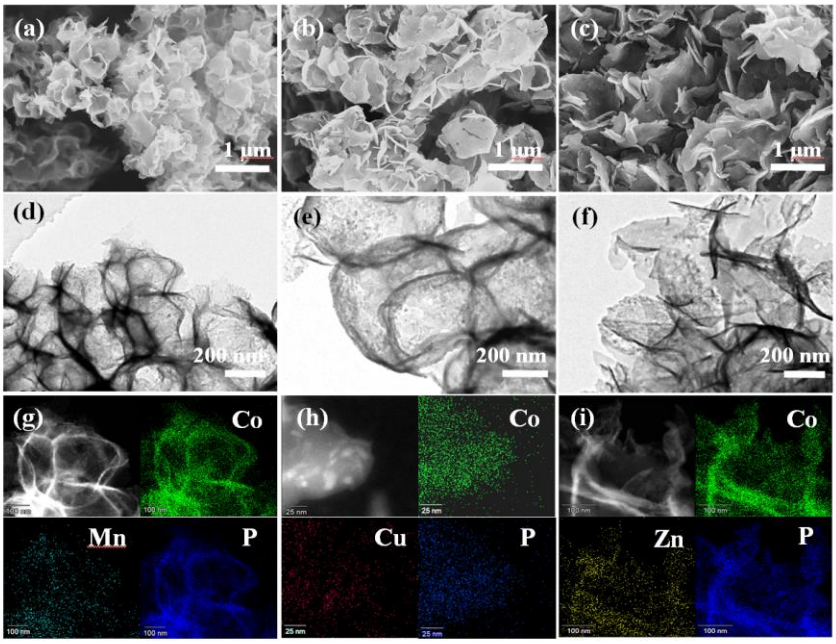

Figure S18. (a) SEM, (d) TEM, and (g) STEM images and elemental mapping data of CoMn(20:1)-P-NS; (b) SEM (e) TEM, and (h) STEM images and elemental mapping data of CoCu(20:1)-P-NS; (c) SEM, (f) TEM, and (i) STEM images and elemental mapping data of CoZn(20:1)-P-NS.

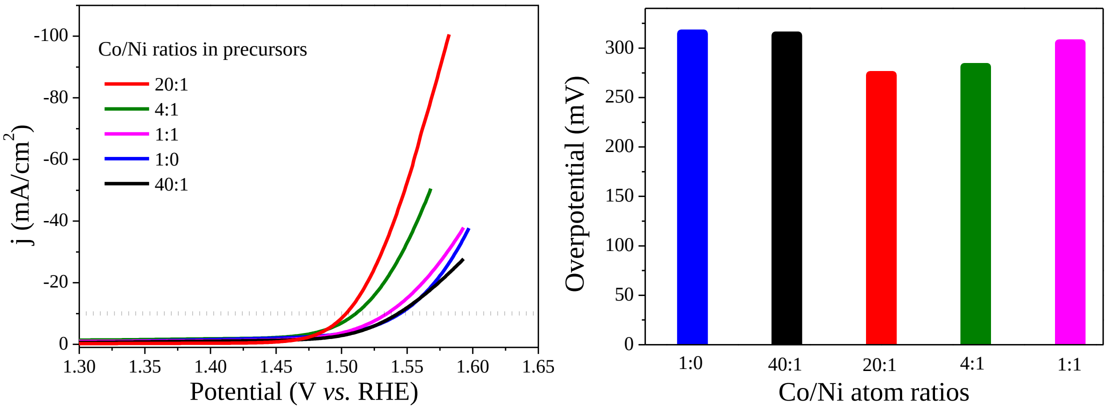

Figure S19. (a) The LSV curves of CoNi-P-NS with different Co/Ni ratios in the starting precursor on a GCE at a rotation speed of 1600 rpm at a scan rate of 10 mV/s in 1.0 M KOH. CoNi-P-NS with a molar ratio of Co/Ni = 20:1 exhibits the optimized OER activity, which gives a lowest overpotential of 273 mV at 10 mA/cm^2. (b) The corresponding overpotentials at current density of 10 mA cm^{-2} for the different samples.

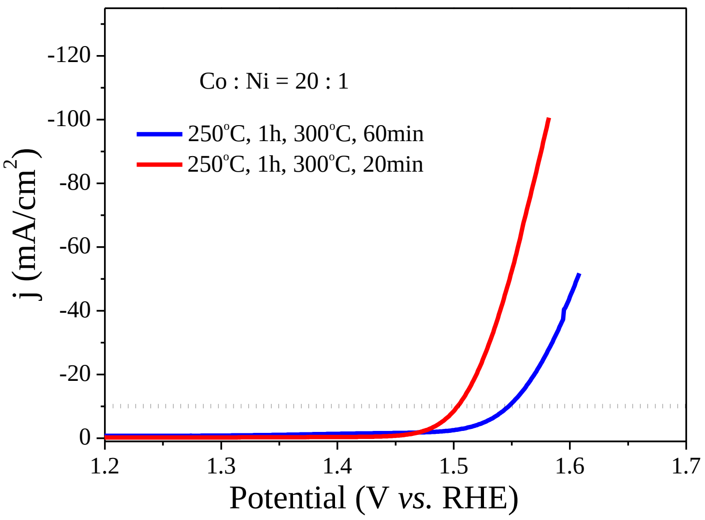

Figure S20. The LSV curves of CoNi(20:1)-P-NS with different phosphidation time at a rotation speed of 1600 rpm at a scan rate of 10 mV/s in 1.0 M KOH.

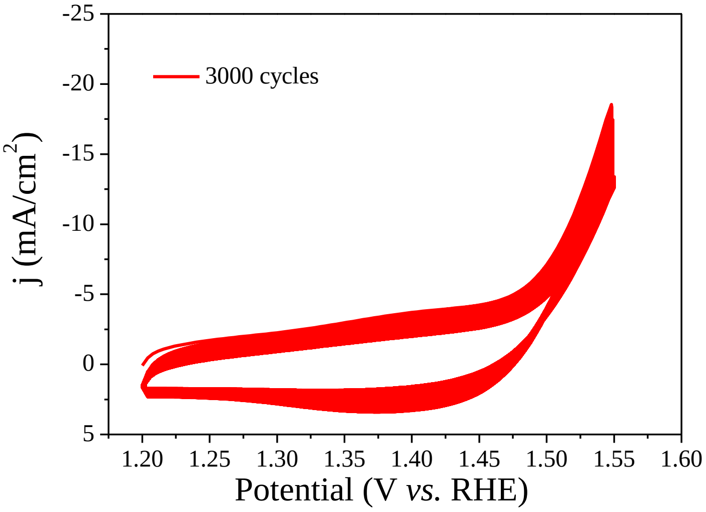

Figure S21. CV curves with 3000 cycles of CoNi(20:)-P-NS at a rotation speed of 1600 rpm at a scan rate of 50 mV/s in 1.0 M KOH

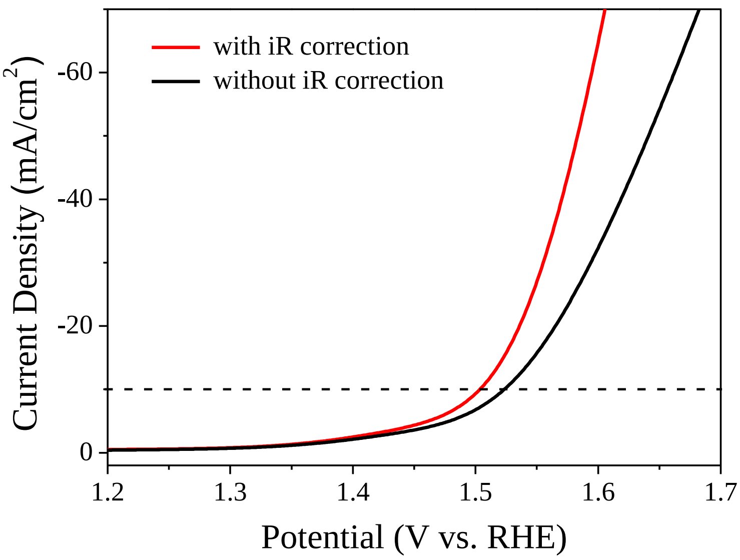

Figure S22. OER polarization curves of CoNi(20:1)P-NS with and without iR correction. In our case, the magnitude of IR corrections was 100%.

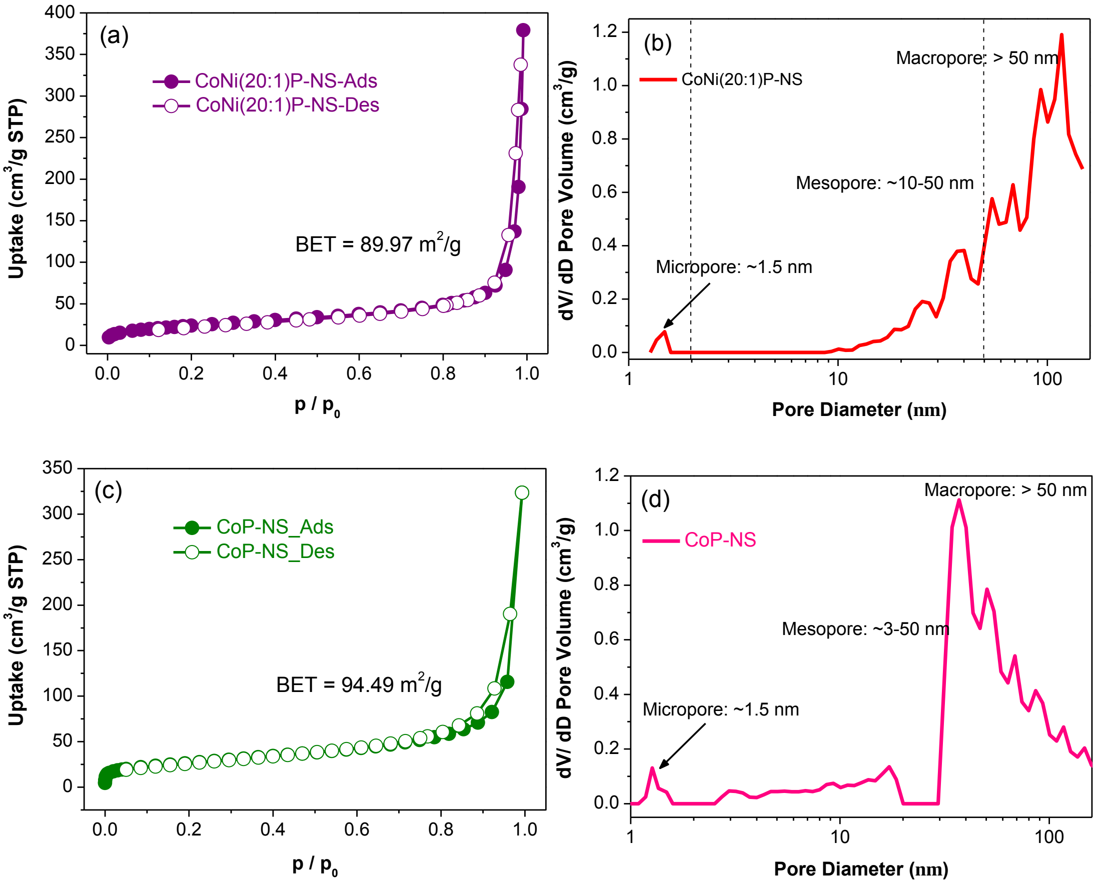

Figure S23. (a) N_2 adsorption/desorption isotherms (b) pore distribution of CoNi(20:1)P-NS; (c) N_2 adsorption/desorption isotherms (d) pore distribution of CoP-NS.

The specific surface area (89.97 m^2/g) for CoNi(20:1)P nanosheets is similar to that of CoP nanosheets (94.49 m^2/g) due to similar material preparation method and similar porous structure and morphology. Our specific surface area is much higher than those of many previously reported other transition metal compounds such as hollow NiP nanoparticles (32.8 m^2/g, J. Am. Chem. Soc. 2013, 135, 9267), Co(OH)F nanowires and CoN_4 porous nanowires (8.85 and 20.75 m^2/g, Angew. Chem. Int. Ed. 2015, 127, 14923).

We have performed N_2 sorption experiments to determine the pore size and distribution. The obtained plot (Figure S23) regarding pore size revealed the presence of micropore (~1.5 nm), mesopore (~10-50 nm) and macropore (> 50 nm) in our CoNi(20:1)P materials. The presence of micropores agrees with TEM observation, which further supports the existence of tiny holes on the plane of nanosheets.

Table S1. OER performances of our sample compared with recently reported representative electrocatalysts.

Catalyst	Electrolytes	Substrate	Overpotential at 10 mA/cm^2 [mV]	Mass loading (mg/cm^2)	Reference
CoNi(20:1)-P-NS	1 M KOH	Ni foam	209	0.153	This work
	1 M KOH	GCE	273	0.153	This work
RuO_2	1 M KOH	GCE	293	0.153	This work
20 wt% Ir/C	1 M KOH	GCE	281	0.153	This work
NiCoP@NF	1 M KOH	Ni foam	280	—	*Nano Lett.* **2016**, 16, 7718.
Fe doped $Ni(OH)_2$/NiOOH /rGO	1 M KOH	GCE	210	0.25	*ACS Nano*, **2015**, 9, 1977
NiFe LDH/CNTs	1 M KOH	Carbon paper	220	0.25	*J. Am. Chem. Soc.* **2013**, 135, 8452
CoOOH	1 M KOH	Glass carbon	300	0.15	*Angew. Chem. Int. Ed.* **2015**, 54, 8722
Co-OEC	1 M KBi	Ni foam	230	0.15	*Energy Environ. Sci.* **2011**, 4, 499
NiFeOx/CFP	1 M KOH	Carbon fiber paper	230	0.60	*Nat. Commun.* **2015**, 6, 7261
α-FeCoOx	1 M KOH	GCE	300	—	*J. Am. Chem. Soc.* **2015**, 137, 3638
NiFe LDH	1 M KOH	GCE	300	0.07	*J. Am. Chem. Soc.* **2015**, 137, 1305
$NiCo_2O_4$	1 M NaOH	Ni foam	290	1.0	*Angew. Chem. Int. Ed.* **2016**, 55, 6290
Co_3O_4/C nanowire arrays	0.1 M KOH	Cu foil	290	—	*J. Am. Chem. Soc.* **2014**, 136, 13925
Co_4N/CC	1 M KOH	Carbon	257	0.82	*Angew. Chem. Int.*

		cloth			*Ed.* **2015**, 54, 14710
N-Co_9S_8/G	0.1 M KOH	GCE	409	0.2	*Energy Environ. Sci.* **2016**, 9, 1320

Table S2. OER performances of our samples compared with recently reported monometallic and bimetallic phosphides.

Catalyst	Electrolytes	Substrate	Overpotential at 10 mA/cm^2 [mV]	Mass loading (mg/cm^2)	Referance
CoNi(20:1)-P-NS	1 M KOH	Ni foam	209	0.153	This work
	1 M KOH	GCE	273	0.153	This work
RuO_2	1 M KOH	GCE	293	0.153	This work
20 wt% Ir/C	1 M KOH	GCE	281	0.153	This work
CoP-NS	1 M KOH	GCE	315	0.153	This work
CoMn(20:1)-P-NS	1 M KOH	GCE	298	0.153	This work
CoCu(20:1)-P-NS	1 M KOH	GCE	281	0.153	This work
CoZn(20:1)-P-NS	1 M KOH	GCE	276	0.153	This work
De-LNiFeP/rGO	0.1 M KOH	Carbon paper	274	0.5	*Energy Environ. Sci.* **2015**, 8, 1719
	0.1 M KOH		282	0.5	
	0.1 M KOH		291	0.5	
	1 M KOH		258	0.5	
	1 M KOH		271	0.5	
	1 M KOH		277	0.5	
Co-P film	1 M KOH	Cu foil	345	1.0	*Angew. Chem. Int. Ed.* **2015**, 54, 6251
$(Co_{0.54}Fe_{0.46})_2P$ sea-urchins	0.1 M KOH	GCE	370	0.204	*Nanoscale* **2016**, *8*, 3244
$(Co_{0.47}Fe_{0.53})_2P$/C sea-urchins	0.1 M KOH	GCE	370	0.204	*Angew. Chem. Int. Ed.* **2015**, 54, 9642
	1 M KOH	GCE	280	0.204	
Co_2P/C NPs	0.1 M KOH	GCE	430	0.204	
Fe_2P/C nanowires	0.1 M KOH	GCE	560	0.204	
CoMnP NPs	1 M KOH	GCE	330	0.284	*J. Am. Chem. Soc.* **2016**, 138, 4006
CoP/C	1 M KOH	GCE	360	0.4	*ACS Catal.* **2015**, 5, 4066
Ni_2P NPs	1 M KOH	GCE	290	0.14	*Energy Environ. Sci.* **2015**, 8, 2347
CoP/rGO-400	1 M KOH	GCE	340	0.28	*Chem. Sci.* **2016**, 7, 1690
Co-P/NC	1 M KOH	GCE	354	0.283	*Chem. Mater.* **2015**,

					27, 7636
CoP hollow polyhedron	1 M KOH	GCE	400	0.102	*ACS Appl. Mater. Inter.* **2016**, 8, 2158
CoP nanorods/C	1 M KOH	GCE	320	0.7	*ACS Catal.* **2015**, 5, 6874
CoP NP/C	1 M KOH	GCE	340	0.7	
PCPTF films	1 M KOH	Au	297	0.1	*Adv. Mater.* **2015**, 27, 3175
CoP nanoneedle	1 M KOH	Carbon Cloth	281	3.3	*ChemSusChem* **2016**, 9, 472
np-$(Co_{0.52}Fe_{0.48})_2P$	1 M KOH	Free-standing	270	NA	*Energy Environ. Sci.* **2016**, 9, 2257
CoP-MNA	1 M KOH	Ni foam	390	NA	*Adv. Funct. Mater.* **2015**, 25, 7337
Sandwich-like CoP/C	1 M KOH	GCE	330	0.36	*J. Mater. Chem. A* **2016**, 4, 9072
CoP-CNT	0.1 M NaOH	GCE	330	0.285	*ACS Appl. Mater. Inter.* **2015**, 7, 28412

Table S3. Ionic radius of various elements in crystals.[3]

Ion	Co^{2+} (hs)	Ni^{2+}	Mn^{2+}	Cu^{2+}	Zn^{2+}
Radius (pm)	74	69	67	73	74

References

[1] J. Yang, F. Zhang, H. Lu, X. Hong, H. Jiang, Y. Wu, Y. Li, *Angew. Chem. Int. Ed.*, **2015**, 54, 10889-10893.

[2] J. Rossmeisl, Z. W. Qu, H. Zhu, G. J. Kroes, J. K. Nørskov, *J. Electroanal. Chem.*, **2007**, 607, 83-89.

[3] Z. F. Huang, J. Song, K. Li, M. Tahir, Y. T. Wang, L. Pan, L. Wang, X. Zhang, J. J. Zou, *J. Am. Chem. Soc.*, **2016**, *138*, 1359-1365.